CHEMISTRY
A EUROPEAN JOURNAL

DOI: 10.1002/chem.200800453

The First Silicon-Based Cationic Clathrate III with High Thermal Stability: $Si_{172-x}P_xTe_y$ ($x = 2y$, $y > 20$)

Julia V. Zaikina,[a, b] Kirill A. Kovnir,[a] Frank Haarmann,[a] Walter Schnelle,[a] Ulrich Burkhardt,[a] Horst Borrmann,[a] Ulrich Schwarz,[a] Yuri Grin,*[a] and Andrei V. Shevelkov*[b]

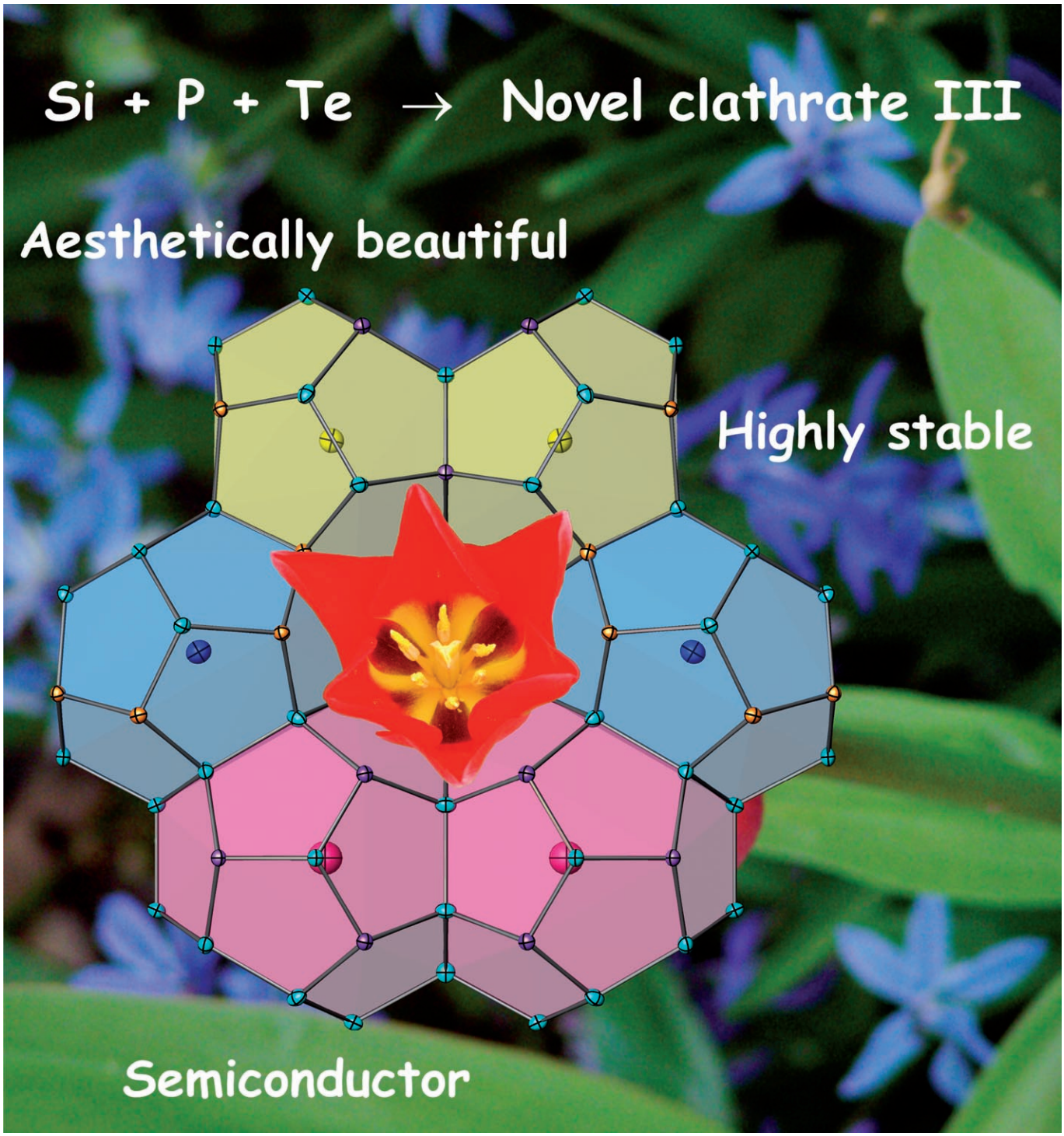

Abstract: A new representative of a very rare clathrate III family, $Si_{130}P_{42}Te_{21}$, has been synthesized from the elements. It crystallizes in the tetragonal space group $P4_2/mnm$ (no. 136) with the unit cell parameters $a=19.2632(3)$ Å, $c=10.0706(2)$ Å. Single crystal X-ray diffraction and solid state ^{31}P NMR revealed a non-random distribution of phosphorus atoms over the framework positions. The crystal structure features a peculiar packing of large polyhedra $Te@(Si/P)_n$ never observed before for cationic clathrates. Despite the structural complexity, the composition of the novel clathrate Is in accordance with the Zintl rule, which was confirmed by a combination of optical metallography, scanning electron microscopy (SEM) and wavelength dispersive X-ray spectroscopy (WDXS), as well as by diamagnetic and semiconducting behavior of the synthesized phase. Clathrate $Si_{130}P_{42}Te_{21}$ exhibits the highest reported thermal stability for this class of materials, it decomposes at 1510 K. This opens new perspectives for the creation of clathrate-based materials for high-temperature applications.

Keywords: cationic clathrates · phosphorus · silicon · solid-state NMR spectroscopy · zintl phases

Introduction

The term "clathrate" refers to compounds comprising host frameworks that embrace guest species in polyhedral cages.[1] The members of this class cover a wide range of chemically different phases, as the four-coordinate species that form the networks may be oxygen of the water molecules, silicon of the building unit $SiO_{4/2}$, neutral atoms, or charged ions.[1,2] Large cages with sizes up to 10 Å are capable of accommodating guest atoms. Owing to non-directed interactions between host and guest, clathrates may be regarded as supramolecular compounds.[1b] The recent impetuous interest in tetrel-type clathrates in which the host framework is based on Si, Ge, or Sn atoms is motivated in particular by the search for a new generation of efficient thermoelectric materials.[3]

Clathrates—gas and liquid hydrates—crystallize in seven structure types notated as I–VII.[1a] Tetrels form clathrate crystal structures of the types I and II plus the variants VIII and IX not known for aqueous phases.[2,4] The chiral clathrate IX (structure type $Ba_6In_4Ge_{21}$[4b]) is sometimes incorrectly referred to as clathrate III, although the latter is originally the tetragonal structure motif of a bromine hydrate $[(Br_2)_{20}\square_{10}](H_2O)_{172}$.[1a,5]

Clathrates can be classified by the charge distribution between the framework and guest. In anionic clathrates, cations of alkali- or alkaline-earth metals, or europium balance the negatively charged framework.[4,6] The tin-based compound $A_{30}Na_{(1.33x-10)}Sn_{(172-x)}$ (A = Cs or Cs/Rb), featuring a pronounced disorder with vacancies at tin sites and a random distribution of sodium atoms within the framework, represents the sole anionic clathrate III-like network containing tetrels.[6]

In the sparse group of so-called inverse or cationic clathrates,[1b,2] the negative charges of halogen or tellurium guest anions are compensated by positive charges of the framework based on Si, Ge, or Sn accompanied by pnicogen, tellurium, or even iodine. $Ge_{38}P_8I_8$[7] was synthesized by von Schnering and Menke and was the first example of a cationic clathrate. Since then a number of germanium- and tin-based cationic clathrates have been prepared,[2] however, only a few silicon-based cationic clathrates are known so far; $Si_{40}P_6I_{6.5}$,[8] $Si_{46-x}P_xTe_y$,[9] $Si_{38}Te_{16}$,[10] and $Si_{44.5}I_{9.5}$.[11] The latter two require high pressure for synthesis, whereas phosphorus-containing clathrates can be prepared at ambient pressure. All hitherto known cationic clathrates belong to the clathrate I type.[2] Here, we present the first cationic clathrate III $Si_{130}P_{42}Te_{21}$, which has high thermal stability and a peculiar crystal structure.

Results and Discussion

Synthesis, X-ray powder data and chemical composition: Initially, $Si_{172-x}P_xTe_y$ was obtained as a by-product in Si-rich samples during the investigation of a homogeneity range of the clathrate I $Si_{46-x}P_xTe_y$.[9] A single crystal of the clathrate III phase was separated from a sample containing both phases, clathrate I and clathrate III. The crystal structure of the clathrate III was determined from X-ray single crystal diffraction data. Subsequently, the clathrate III was synthesized with a composition $Si_{130}P_{42}Te_{21}$ in 100% yield by using optimized preparation conditions. X-ray powder diffraction revealed no evidence for impurity phases in the synthesized sample. Thorough metallographic, scanning electron microscopy (SEM) and wavelength dispersive X-ray spectroscopy (WDXS) investigations confirmed that the synthesized sample of clathrate III is a single phase (Figure 1) with the

[a] Dipl.-Chem. J. V. Zaikina, Dr. K. A. Kovnir, Dr. F. Haarmann, Dr. W. Schnelle, Dr. U. Burkhardt, Dr. H. Borrmann, Dr. U. Schwarz, Prof. Yu. Grin
Max-Planck-Institut für Chemische Physik fester Stoffe
Nöthnitzer Straße 40, 01187 Dresden (Germany)
Fax: (+49) 351-4646-4002
E-mail: grin@cpfs.mpg.de

[b] Dipl.-Chem. J. V. Zaikina, Prof. Dr. A. V. Shevelkov
Chemistry Department, Lomonosov Moscow State University
Leninskie Gory 1–3, 119991 Moscow (Russia)
Fax: (+7) 495-939-4788
E-mail: shev@inorg.chem.msu.ru

Supporting information for this article is available on the WWW under http://www.chemeurj.org/ or from the author.

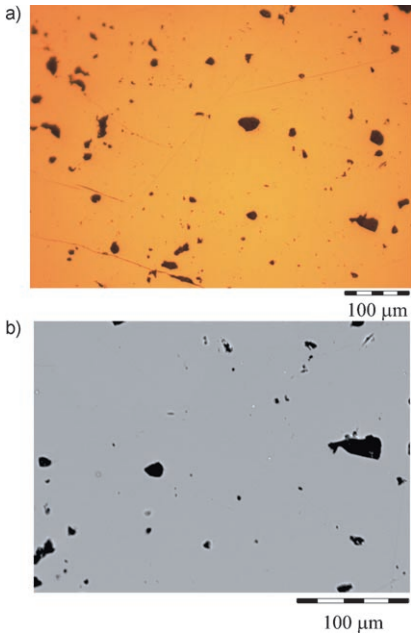

Figure 1. Single-phase microstructure of $Si_{130}P_{42}Te_{21}$; a) bright-field image, b) back scattering electron image. Dark areas correspond to holes in the sample.

composition $Si_{130.0(2)}P_{42.0(1)}Te_{21.0(2)}$ normalized to the 172 framework Si and P atoms. Additionally, the composition was corroborated by density measurements: $\rho_{exptl} = 3.352(9)\ g\,cm^{-3}$ that is 99% of $\rho_{calcd} = 3.39(1)\ g\,cm^{-3}$ calculated by using the composition determined by the WDXS analysis and the unit cell parameters taken from X-ray powder data.

Analysis of the crystal structure showed that the clathrate framework is vacancy-free, whereas one of the guest Te positions is only partially occupied. The investigation of the homogeneity range of $Si_{172-x}P_xTe_y$ ($x = 2y$, $19 \le y \le 23$) revealed that single-phase samples of clathrate III can be obtained only for $20 \le y \le 22$. In case of $y = 23$ only clathrate I $Si_{46-x}P_xTe_{6.4(1)}$ was formed.[12] Lowering y to 19 resulted in the formation of clathrate III with a considerable admixture of elemental silicon. More precise determination of the homogeneity range of clathrate III is a subject of further investigations.

Crystal structure determination: The crystal structure of $Si_{130}P_{42}Te_{21}$ was solved in the space group $P4_2/mnm$ (no. 136) by direct methods[13] that allowed the localization of all atomic positions of the crystal structure. During the initial steps of the refinement all framework atoms were treated as Si while the guest atoms were set as Te by analogy with clathrate I $Si_{46-x}P_xTe_y$.[9] The subsequent refinement showed that atomic displacement parameters (ADPs) for the Te(1) and Te(4) atoms were notably larger than those for the other two Te atoms. Occupancies of these atoms were allowed to vary. It turned out that the occupancy of the position Te(4) was ≈15%, although the occupancy for Te(1) did not deviate significantly from unity. Fixing the ADPs for the Te(4) atom to different values (to the same ADPs as for other Te atoms or to a half of freely refined parameters) allowed us to estimate the uncertainties in the occupancy determination. Finally, the site occupancy factor (SOF) of Te(4) was found to be 0.15(2).

At the next step, the occupancies of all framework atoms set as Si (positions are marked by X(1) to X(17) in Table S1 in the Supporting Information) were refined simultaneously to 100% except for X(1) and X(2) in which they slightly exceeded unity. This allowed us to conclude that there are no vacancies at the framework positions. Although the X-ray data were available up to high diffraction angles (Table 1), it was not possible to refine mixed Si/P occupancies at individual sites. The assignment of the phosphorus atoms in the framework was thus based on the analysis of interatomic distances (Table S1) revealing two relatively short distances of 2.26 Å (X(1)–X(13) and X(2)–X(13)), which can be assigned to P–Si distances.[9b] However, the distances of 2.33 Å between symmetrically equivalent X(13) sites are relatively long. Therefore X(13) is considered to be an Si site. In accordance with the occupancy refinement and the distance analysis the positions X(1) and X(2) were assigned as fully occupied by phosphorus atoms. Based on the distance criteria the X(3), X(4) and X(5) positions were considered to have mixed occupation by 45% P and 55% Si.[9b] The amount of P in these positions was calculated based on the assumption that the phosphorus content in the crystal structure corresponded to twice the tellurium content (vide infra). Distances between the other 12 framework positions were significantly larger (>2.31 Å), and all these positions were set as fully occupied by Si. All atoms in the crystal structure were refined using anisotropic ADPs.

Special care was taken to uncover the reason for the relatively high ADPs for Te(1). Actually, it is typical for clathrates that a guest atom in a larger cage has higher ADPs

Table 1. Data collection and structure refinement parameters for $Si_{130}P_{42}Te_{21.2}$.

composition	$Si_{130}P_{42}Te_{21.2(2)}$
space group	$P4_2/mnm$ (no. 136)
M_r [g mol^{-1}]	7657.56
cell parameters [Å]	$a = 19.2573(6)$[a]
	$c = 10.0525(7)$[a]
V [Å^3]	3727.9(3)
T [K]	295(2)
Z	1
radiation, λ [Å]	$Ag_{K\alpha}$, 0.56085
ρ_{calc} [g cm^{-3}]	3.411
μ [mm^{-1}]	2.926
θ range [°]	$2.36 < \theta < 27.86$
refl. collected	52879
independent refl.	4867 [$R_{int} = 0.095$]
data/param.	4867/137
R_1, wR_2 [$I > 2\sigma(I)$]	0.045,[b] 0.128[c]
goodness-of-fit on F^2	1.060

[a] Powder data. [b] $R_1 = \Sigma\,|F_o| - |F_c|\,/\Sigma\,|F_o|$. [c] $wR_2 = [\Sigma w(F_o^2 - F_c^2)^2/\Sigma w(F_o^2)^2]^{1/2}$, $w = [\sigma^2(F_o^2) + (A \cdot p)^2 + B \cdot p]^{-1}$; $p = (F_o^2 + 2F_c^2)/3$; $A = 0.1039$; $B = 0.2764$.

than guest atoms residing in smaller cages. For example, in the type I clathrate $Si_{46-x}P_xTe_y$, the ratio of U_{eq} for Te atoms in the 20-vertex and 24-vertex cages is 1:2.[9b] One may expect that in the larger 26-vertex cage, the ADPs of the guest atoms can be even larger. The Fourier difference maps around this position (Figure S1 in the Supporting Information) showed that the electron density exhibited only one pronounced maximum in the 4*f* position (0.4015; *x*; 0). Refinement of the respective site occupancy did not reveal deviations from unity. Refinement with artificially reduced and fixed ADPs led to a slight decrease of the occupancy, however, at the cost of a significant increase in *R*-values and appearance of high residual peaks in the difference map around the Te(1) position. Thus, it was concluded that this position is fully occupied.

Table 2. Atomic coordinates and equivalent isotropic displacement parameters [Å^2] for $Si_{130}P_{42}Te_{21.2}$. U_{eq} is defined as one third of the trace of the orthogonalized U_{ij} tensor.

Atom	Site	*x*/*a*	*y*/*b*	*z*/*c*	U_{eq}
Te(1)	4*f*	0.40148(3)	*x*	0	0.0245(1)
Te(2)	8*j*	0.18157(1)	*x*	0.24658(5)	0.0136(1)
Te(3)	8*i*	0.13029(2)	0.46638(2)	0	0.0140(1)
Te(4)[a]	8*i*	0.0666(1)	0.7472(1)	0	0.0104(8)
P(1)	8*j*	0.31454(5)	x	0.3164(1)	0.0063(3)
P(2)	16*k*	0.00226(6)	0.13448(6)	0.1848(1)	0.0062(1)
E(3)[b]	8*i*	0.07116(9)	0.15537(9)	0	0.0088(3)
E(4)[b]	16*k*	0.04963(6)	0.31734(6)	0.1835(1)	0.0055(2)
E(5)[b]	16*k*	0.13303(6)	0.36547(6)	0.3165(1)	0.0060(2)
Si(6)	4*g*	0.40659(9)	0.59341(9)	0	0.0067(4)
Si(7)	4*d*	0	1/2	1/4	0.0059(4)
Si(8)	4*g*	0.23758(9)	0.76242(9)	0	0.0069(4)
Si(9)	8*i*	0.10554(9)	0.27051(9)	0	0.0067(3)
Si(10)	8*i*	0.29046(9)	0.55877(9)	0	0.0062(3)
Si(11)	8*j*	0.22129(9)	0.30684(9)	0	0.0062(3)
Si(12)	8*j*	0.04295(6)	*x*	0.3137(1)	0.0073(3)
Si(13)	8*i*	0.39378(6)	*x*	0.3842(1)	0.0066(3)
Si(14)	16*k*	0.20613(9)	0.64601(9)	0	0.0060(3)
Si(15)	16*k*	0.26477(6)	0.49226(6)	0.1875(1)	0.0075(2)
Si(16)	16*k*	0.23350(6)	0.37497(6)	0.1894(1)	0.0070(2)
Si(17)	16*k*	0.02557(6)	0.59543(6)	0.1167(1)	0.0061(2)

[a] SOF = 0.15(2). [b] Mixed Si/P positions (0.55/0.45) are denoted as E.

A model with a Te(1) split position was also refined: a tellurium atom was shifted from an ideal 4*f* position into a position 8*j* with 50% occupancy (0.4015; *x*; −0.0112). This model led to a similar description of the electron density with a smaller Te(1) ADP along [001], as expected. No crystal-chemical reasons for such a splitting were found, e.g., significant shortening of guest-framework distances; the shortest Te(1)–Si distance exceeded 3.4 Å. The next model considered the Te(1) atom in the ideal 4*f* position, but with anharmonic atomic displacement parameters.[14] All models converged to a composition with one tellurium atom per 26-vertex cage. Thus, the simplest model with Te(1) occupying the ideal 4*f* position and anisotropic ADPs was chosen for further evaluation.

The final refinement using anisotropic displacement parameters for all atoms led to the composition $Si_{130}P_{42}Te_{21.2(2)}$ with $R_F = 0.045$. The details of refinement, final atomic parameters, and selected interatomic distances are presented in Tables 1–3, respectively.

Table 3. Selected interatomic distances [Å] for $Si_{130}P_{42}Te_{21.2}$.

Atoms	Distance	Atoms	Distance
P(1)–Si(8)	2.328(2)	E(5)–Si(16)	2.326(1)
P(1)–Si(13)	2.263(2)	E(5)–Si(17)	2.319(1)
P(1)–Si(16)	2.328(1)	Si(6)–Si(10)	2.334(2)
P(2)–E(3)	2.318(1)	Si(6)–Si(12)	2.323(2)
P(2)–Si(12)	2.324(1)	Si(7)–Si(17)	2.327(1)
P(2)–Si(13)	2.268(1)	Si(8)–Si(14)	2.322(2)
P(2)–Si(15)	2.335(1)	Si(9)–Si(11)	2.336(2)
E(3)–E(3)	2.293(3)	Si(10)–Si(14)	2.337(2)
E(3)–Si(9)	2.314(2)	Si(10)–Si(15)	2.332(1)
E(4)–E(5)	2.286(1)	Si(11)–Si(11)	2.324(3)
E(4)–Si(9)	2.319(1)	Si(11)–Si(16)	2.324(1)
E(4)–Si(15)	2.324(1)	Si(12)–Si(12)	2.339(3)
E(4)–Si(17)	2.318(1)	Si(13)–Si(13)	2.327(4)
E(5)–Si(14)	2.317(1)	Si(15)–Si(16)	2.338(1)
		Si(17)–Si(17)	2.327(1)

Description of the crystal structure: The atomic arrangement of $Si_{172-x}P_xTe_y$ corresponds to that of clathrate III and is generally analogous to the bromine hydrate $[(Br_2)_{20}\square_{10}]$-$(H_2O)_{172}$.[1a,5] 172 four-coordinate Si and P atoms build the host framework with the cages filled by Te atoms. Three types of polyhedral cages can be distinguished (Figures 2 and 3). All have twelve pentagonal faces, but they differ in the number of hexagonal faces, and therefore in size: a 20-vertex cage [5^{12}], a 24-vertex cage [$5^{12}6^2$], and a 26-vertex cage [$5^{12}6^3$].[15] The cages occur in the ratio 10:16:4 resulting in 30 cavities per unit cell available for the guest Te atoms (Figure 2g and Figure 3b). Cages [$5^{12}6^2$] form two types of columns along [001], single or four-condensed. The first type of the column is formed by sharing the hexagonal faces, similar to clathrate I (Figure 2a). In the (001) plane, the columns are inter-connected by single Si–Si bonds (Figure 2b). Further, the large square-shaped channels are filled by another type of 24-vertex cage column (Figure 2d) composed of coupled cages joined in such a way that every other pair is rotated by 90°, forming the column running along [001] (Figure 2c). The remaining space is filled by isolated pairs of large [$5^{12}6^3$] and small [5^{12}] cages (Figure 2e,f) resulting in formation of the dense packed arrangement (Figure 2g).

Analogous to the aristotype - bromine hydrate - only the large 24- and 26-vertex cages are fully occupied in

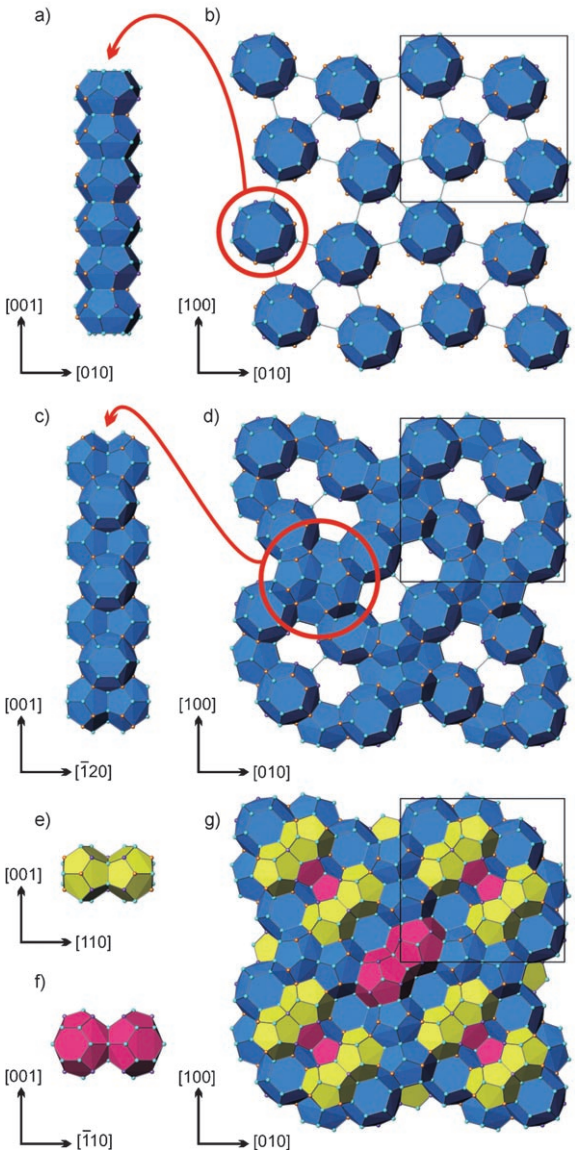

Figure 2. Polyhedral packing in the clathrate III-type structure. a–d) Arrangements of 24-vertex cages, e–f) coupled 26-vertex and 20-vertex cages and g) total polyhedral representation of the structure.

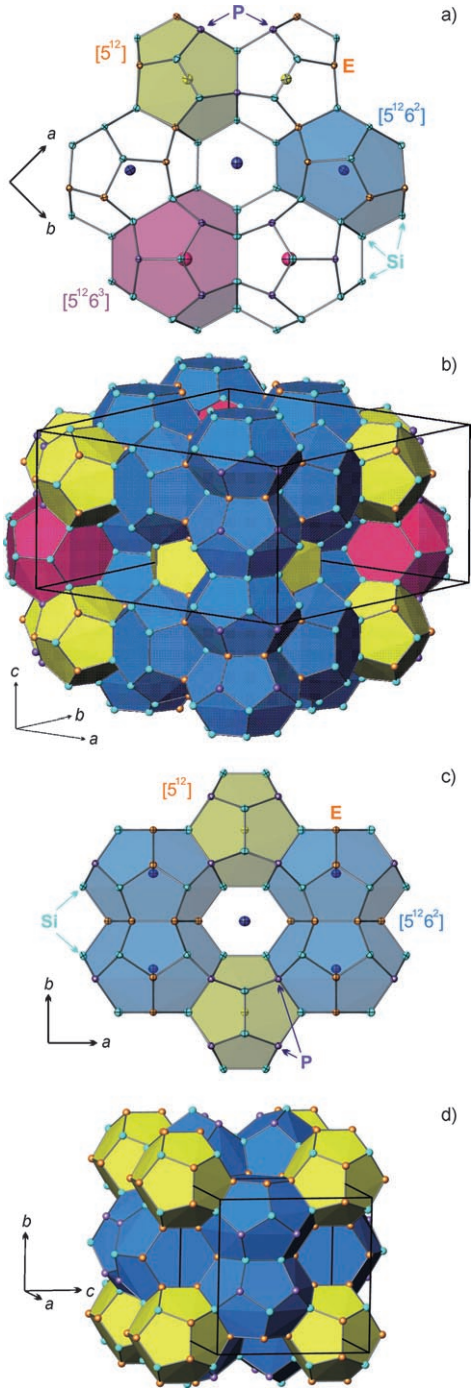

Figure 3. Comparison of the crystal structures of cationic Si–P–Te clathrates: a,b) clathrate III $Si_{172-x}P_xTe_y$, c,d) clathrate I $Si_{46-x}P_xTe_y$.[9b] The 20-vertex cages [5^{12}] the 24-vertex cages [$5^{12}6^2$] and the 26-vertex cages [$5^{12}6^3$] are shown as yellow, blue and pink polyhedra, respectively. Phosphorus, violet; silicon, cyan; E (mixed Si/P), orange. Thermal ellipsoids in a) and c) are shown with 90% probability.

$Si_{172-x}P_xTe_y$, while eight of the ten 20-vertex cages are partially filled (≈15%) and two others are empty. A similar trend was observed for the clathrate I phase $Si_{46-x}P_xTe_y$[9] (Figure 3c,d) in which Te atoms fully occupy a 24-vertex cage, and only partially fill a 20-vertex cage, which is similar to other silicon clathrates I, $K_{7.62(1)}Si_{46}$ and $Rb_{6.15(2)}Si_{46}$,[16] in which the size of the guest atoms defines the population of the small cage by guest atoms. Apparently, an occupation of the smaller $(Si/P)_{20}$ dodecahedral [5^{12}] cage is disadvantageous for the large Te guest anions, especially in case of high phosphorus concentrations. Furthermore, the Te atoms in the 26-vertex cages have an ADP value two times larger than those of the Te atoms located in the 20- and 24-vertex cages. Typically, for clathrates, the large ADP values for the guest atoms are generally found to be consistent with abnormally low thermal conductivity, which originate from the scattering of phonons at rattling (vibrating) guest atoms and are responsible for their high thermoelectric efficiency.[3]

In the crystal structures of clathrate I and clathrate III (Figure 3), similar columns of the 24-vertex cages [$5^{12}6^2$] are

formed by sharing the hexagonal faces. However, in case of clathrate I, small pentagonal dodecahedra [5^{12}] are isolated and surrounded only by large cavities [$5^{12}6^2$], whereas in clathrate III, all cages are condensed (Figure 2 and 3a,b). Analysis of the Si/P distribution within the frameworks of both clathrate I $Si_{46-x}P_xTe_y$[9] and clathrate III $Si_{172-x}P_xTe_y$ reveals that phosphorus atoms mainly form small 20-vertex [5^{12}] cages and tend to avoid common hexagonal faces of the large polyhedra [$5^{12}6^2$] and/or [$5^{12}6^3$] (Figure 3a,c). The hexagonal rings are formed by the most "stressed" atoms because their bond angles deviate considerably from the regular tetrahedral values. Implementation of the small phosphorus atoms ($r_{cov}(P) < r_{cov}(Si)$) to these rings appears to be energetically unfavorable. A similar behavior was observed for boron in the anionic clathrate I $K_7B_7Si_{39}$.[4h]

The crystal structure of the earlier reported anionic clathrate III $A_{30}Na_{(1.33x-10)}Sn_{(172-x)}$ (A = Cs, Cs/Rb)[6] differs distinctly from $Si_{172-x}P_xTe_y$. Here, the cages are completely filled by the A^+ cations, although, vacancies are formed in the host framework and additional Na atoms stabilize the whole structure, filling up the space of the missing Sn_2 pairs. The stabilization of the clathrate III-type structure was mainly attributed to this sodium "substitution" in the framework.[6] A completely different type of stabilization is observed in the crystal structure of $Si_{172-x}P_xTe_y$. The host framework does not contain vacancies, but some of the silicon atoms are substituted by phosphorus atoms in order to attain charge balance. According to the Zintl concept,[17] four-coordinate silicon atoms are neutral, whereas four-coordinate phosphorus complies with P^+, analogous to $Ge_{38}P_8I_8$.[7] In turn, the tellurium guest atoms, forming no covalent bonds with framework, can be written as Te^{2-}. Thus, the electron-balanced composition of clathrate III may be written as $(Si^0)_{172-x}(P^+)_x(Te^{2-})_y$ ($x = 2y$). Moreover, the cationic clathrate III features a homogeneity range owing to slight variations in the occupation of the 20-vertex cages by tellurium, although the overall composition is expected to follow the Zintl count. The increase in the Te occupation of the cages leads to a higher P content within the framework, and to its corresponding compression, similar to the findings for the cationic clathrate I.[9]

^{31}P NMR spectroscopy: Additional evidence for structurally different phosphorus atoms in $Si_{172-x}P_xTe_y$ ($x = 42$; $y = 21$) is obtained by the solid state NMR. The observed ^{31}P NMR signal is in the range $\delta = -300$–200 ppm, similar to other cationic clathrates.[18a] The small and mainly negative shift of the signal indicates orbital contributions, regarding chemical shielding as an origin of the signal shift. A typical range $\delta = -400$–600 ppm is observed in non-conducting diamagnetic compounds.[18b] The static ^{31}P NMR wide-line signal shows a featureless line shape (Figure 4, top). The width of the individual contributions used to describe the signal is relatively large compared to well ordered compounds such as M_4Si_4 with M = Na, K, Rb, Cs.[19] This is an additional evidence of the intrinsic disorder of the compound resulting in similar, but slightly different shifted signals, as described by continuous distributions of shifts for fitting of the signal. Magic angle spinning (MAS) results only in a small reduction of the line width and two separated intensity maxima and a shoulder at high frequencies become visible (Figure 4, top). This indicates that the signal is composed by at least three main contributions. Using the intensity ratio 18:16:8 taken from the X-ray diffraction data, the line shape of the MAS signal can be described quite satisfactorily (Figure 4, top). More narrow contributions indicating a minor influence of disorder are assigned to P(1) and P(2), whereas a broad signal contribution is assigned to the sites E(3), E(4), and E(5) with the mixed occupation of P and Si.

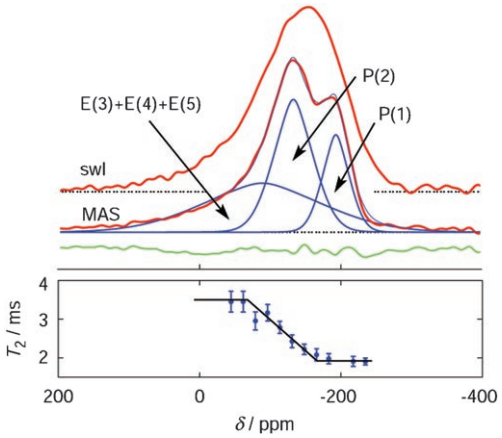

Figure 4. ^{31}P NMR signals of $Si_{130}P_{42}Te_{21}$ (top) measured at ambient temperature and $B_0 = 11.74$ T. The static wide line spectrum (swl) and the MAS spectrum with a rotation frequency of 35 kHz are normalized and separated by an arbitrary offset (red lines). The individual contributions obtained by least-squares fitting of the MAS signal and the difference of the observed and simulated total signal are indicated in blue and green, respectively. Spin–spin relaxation time (bottom) T_2 obtained from frequency dependent selective excitation experiments. The black line is a guide to the eye.

The model used to describe the line shape of the NMR signal is supported by spin–spin relaxation experiments. These are sensitive to the local environment of the nuclei since the homonuclear dipole–dipole coupling can be reduced to individual signal contributions by the application of the selective excitation. The spin–spin relaxation time T_2 increases by a factor of at least three upon the application of selective excitation compared to non-selective excitation. Characteristic frequency dependence (Figure 4, bottom) is observed in the selective excitation experiments. Low values of T_2 indicate small average distances of the interacting spins as observed at low frequency. The high values of observed T_2 at large frequencies denote a larger average distance of the interacting nuclei. The change from low to high values of T_2 is a result of the varying intensity of the different signal contributions. The constant high value at high frequencies is in agreement with the large average distance of the nuclei at the mixed sites, E(3), E(4), and E(5).

Physical properties: A sample with the composition $Si_{130}P_{42}Te_{21}$ reveals the diamagnetic behavior ($\chi_0 = -2.4\times$

10^{-3} emu mol^{-1})[20] and exhibits the activated behavior of the conductivity of a semiconductor with a room temperature value of 5×10^{-4} Ω·m (Figure 5) confirming that the phosphorus content corresponds essentially to twice the Te content. We consider these experimental findings as a sufficient evidence to assign $Si_{172-x}P_xTe_y$ ($x=2y$) to the group of Zintl phases fulfilling the $8-N$ rule.

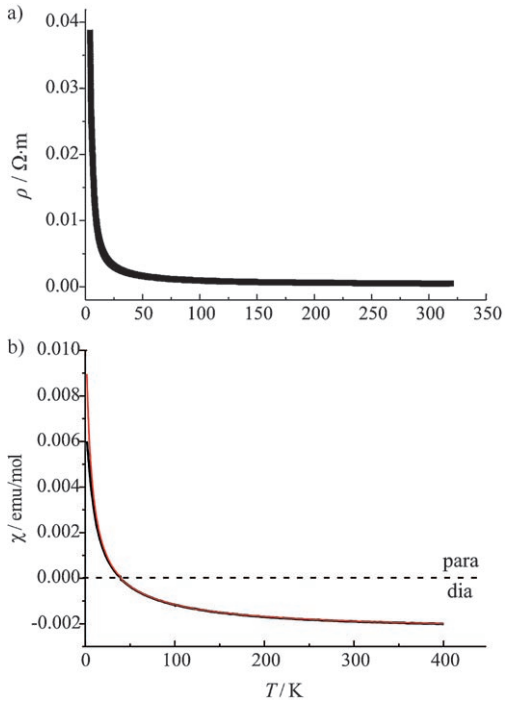

Figure 5. Temperature dependence of the a) electrical resistivity and b) the magnetic susceptibility for $Si_{130}P_{42}Te_{21}$ (7 T, ——; 3.5 T, ——).

Thermal behavior: $Si_{130}P_{42}Te_{21}$ decomposes in vacuum incongruently at the unusually high temperature of 1510 K forming clathrate I and silicon (Figure 6) according to Equation (1). The Te content of the resulting clathrate I was determined by Rietveld refinement of the X-ray powder diffraction data.[12] Because the refinement did not enable us to distinguish P and Si, the clathrate I was specified as a Zintl phase, namely, that the P content is equal to twice the Te content.

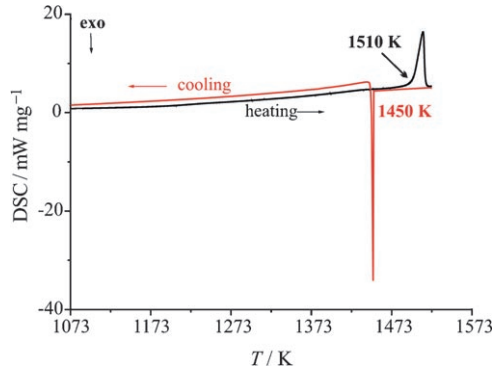

Figure 6. Thermal behavior of $Si_{130}P_{42}Te_{21}$ in vacuum.

$$Si_{130}P_{42}Te_{21} \rightarrow 21.1\,Si + 3.28\,Si_{33.2}P_{12.8}Te_{6.4} \quad (1)$$

Moreover, $Si_{172-x}P_xTe_y$ is stable in air up to 1500 K, without decomposition or oxidation as revealed by X-ray powder diffraction. Its thermal stability exceeds that of other clathrates (Figure 7, Table S2 in the Supporting Information). The decomposition temperatures within chemically related groups of clathrates increase with the absolute value of the electronegativity difference between the framework and the guest atoms ($|\chi_{host}-\chi_{guest}|$).[21] These findings confirm the importance of the charge transfer for the stabilization of clathrate structures.

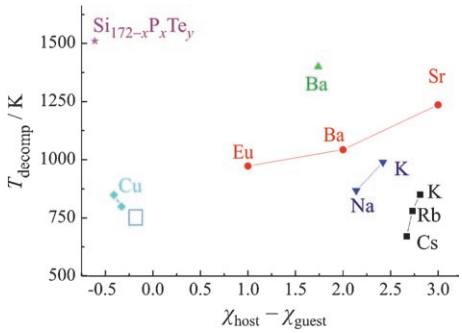

Figure 7. Decomposition temperatures of anionic and cationic clathrates vs. difference between the average electronegativities[21] of the guest and the framework atoms. A_8Sn_{44}, ■; $A_8Ga_{16}Ge_{30}$, ●; $A_8Al_{14}Si_{31}$, ▲; $A_{8-x}Si_{46}$, ▼; $Sn_{24-x}E_xAs_{22}I_8$, ◆; Si–P–Te, ⋆. The lines are guides for the eyes only.

Conclusion

The new cationic clathrate III $Si_{130}P_{42}Te_{21}$ was synthesized from the elements at 1425 K as a single phase. It features a complex crystal structure comprising large polyhedral (Si/P) cages trapping Te anions. Single crystal X-ray diffraction and solid state ^{31}P NMR revealed a non-random distribution of phosphorus atoms over the framework positions. $Si_{130}P_{42}Te_{21}$ is a diamagnetic semiconductor, and therefore a Zintl phase. The obtained clathrate III shows the highest decomposition temperature in vacuum among all reported clathrates: 1510 K. Moreover, the title phase is stable against oxidation in air up to 1500 K. A combination of Si–P framework and Te guest atoms shows a high potential in clathrate chemistry and may serve as a basis for the creation of new clathrate-based materials. The Si–P framework is quite flexible and a significant compression can be achieved by changing the chemical composition. The high thermal stability of the reported phase opens perspectives for high-temperature applications of Si–P frameworks in general and of Si–P–Te clathrates in particular.

Experimental Section

Synthesis and characterization: The stoichiometric mixture of elemental silicon, red phosphorus, and tellurium (the total mass ≈1 g) was heat-treated in a vacuum-sealed quartz ampoule at 1425 K for 18 days, and then cooled quickly by removing the ampoule from the hot furnace. Clathrate III appears as a shiny gray, metal-like dense sinter. According to X-ray powder diffraction (Huber G670 Image Plate Camera, $Cu_{K\alpha_1}$, $\lambda =$ 1.540598 Å, LaB_6, $a = 4.15692$ Å as an internal standard) the sample $Si_{130.0(2)}P_{42.0(1)}Te_{21.0(2)}$ contains single phase clathrate III with the refined unit cell parameters $a = 19.2632(3)$ Å, $c = 10.0706(2)$ Å (least-squares fits, WinCSD software[22]).

Metallographic, SEM and WDXS investigations: Samples for metallographic investigations were prepared by grinding and polishing under inert conditions in an argon glove box.[23] Homogeneity of the microstructures and phase distribution were examined by optical microscopy (Zeiss Axioplan2) in bright field and polarized light contrast and by material contrast images recorded by the back-scattered electron detector at the electron microprobe. Quantitative analysis was performed on a microprobe by the WDXS method (Cameca SX100). GeTe was used to calibrate the tellurium content. For determination of phosphorus and silicon, the binary phase SiP_2 was used as a reference. The individual contributions resulted in a mass concentration residue smaller than 0.5 wt% in the average of ten measurements and leads to the composition $Si_{130.0(2)}P_{42.0(1)}Te_{21.0(2)}$, normalized to 172 framework atoms Si + P.

Crystal structure determination: RIGAKU Spider diffractometer with a rotating anode and Varimax optics, $Ag_{K\alpha}$ radiation, $\lambda = 0.56085$ Å, ω scans, $2\theta_{max} = 55.7°$, 52879 measured, 4867 independent reflections. Absorption correction was performed by a multiscan procedure. Crystal structure refinement was made against F^2 with the program package SHELX-97.[13] Further details of the crystal structure determination may be obtained from the Fachinformationszentrum Karlsruhe, 76344 Eggenstein-Leopoldshafen (Fax: (+49) 7247–808–666, E-mail@fiz-karlsruhe.de), reference number CSD-418901.

NMR spectroscopy: ^{31}P MAS and static wide line (swl) NMR experiments were done using a Bruker AVANCE spectrometer with $B_0 =$ 11.74 T equipped with standard Bruker MAS probes. The sample was mounted in 4 and 2.5 mm zirconium dioxide rotors for spinning frequencies below and above 15 kHz, respectively. A Hahn echo sequence was used in all experiments with an inter pulse delay of 60 μs in swl- and synchronized with rotor frequency in MAS experiments. π pulses of 3 and 200 μs were used in non-selective and selective excitation experiments, respectively. Repetition time of 5 s was sufficient to ensure full recovery of the longitudinal magnetization. The signal shift is referred to H_3PO_4.

Magnetization and electrical resistivity: Magnetization was measured at various external fields between 10 mT and 7 T (1.8–400 K) in a SQUID magnetometer (MPMS XL-7, Quantum Design) on a polycrystalline sample ($m = 171$ mg). The contribution of the sample holder was subtracted. The magnetic susceptibility $\chi(T,H)$ is weakly temperature-dependent and negligibly field-dependent. The upturn of $\chi(T)$ towards low T is owed to traces of paramagnetic impurities or defects (<0.2% of $S = {}^1/_2$ species). χ_0 was calculated from the fit of the curve $\chi(T)$ according to a modified Curie–Weiss law, and found to be $-2.4 \cdot 10^{-3}$ emu mol^{-1}.[20]

The electrical resistivity measurements were performed on a cuboid-shaped sintered sample (1 mm × 1.05 mm × 0.95 mm) with density of 3.287(9) g cm^{-3} that is 97% from the theoretical density. Conventional *dc* four-point method, 4–320 K; inaccuracy of absolute values is estimated to be ±20% owing to the irregular shapes of the investigated samples and resulting problems in determination of the contact geometry.

Thermal behavior: Differential scanning calorimetry (DSC) investigation of the sample $Si_{130}P_{42}Te_{21}$ was performed with the Netzsch DSC 409C equipment in a quartz glass crucible sealed under vacuum or in the open quartz crucible (static air) in the temperature range 300–1520 K with a heating rate of 5 K min^{-1}. After cooling with the same rate, the sample was examined by X-ray powder diffraction.

Density measurements: The density of $Si_{130}P_{42}Te_{21}$ was determined by analyzing the volume of crude powder of a single-phase sample (mass $m =$ 0.1578(1) g) with a helium gas pycnometer (AccuPyc 1330, Micromeritics). Both pycnometer and balance were situated in a glove box filled with argon. The measured volume of $V = 0.0471(1)$ cm^{-3} corresponds to the density $\rho_{exptl} = 3.352(9)$ g cm^{-3} that is in agreement with the density $\rho_{calcd} = 3.39(1)$ g cm^{-3}.

Acknowledgements

J. V. Z. acknowledges the Max-Planck-Gesellschaft for the research fellowship. The authors express their gratitude to Mr. T. Vogel and Ms. M. Eckert for the metallographic and WDXS analyses; Mr. R. Koban for the physical measurements; Ms. S. Müller and Dr. S. Hoffmann for DSC investigation. This work has been supported in part by the Russian Foundation for Basic Research (grants 06–03–32183 and 07–03–12155).

[1] a) G. A. Jeffrey in *Inclusion Compounds* (Eds: J. L. Atwood, J. E. D. Davies, D. D. MacNicol), Academic Press, London, **1984**; b) A. Müller, H. Reuter, S. Dillinger, *Angew. Chem.* **1995**, *107*, 2505–2539; *Angew. Chem. Int. Ed. Engl.* **1995**, *34*, 2328–2361.

[2] a) K. A. Kovnir, A. V. Shevelkov, *Russ. Chem. Rev.*, **2004**, *73*, 923–938; b) S. Bobev, S. C. Sevov, *J. Solid State Chem.* **2000**, *153*, 92–105.

[3] G. A. Slack in *CRC Handbook of Thermoelectrics* (Ed: D. M. Rowe), CRC Press, Boca Raton, FL, **1995**.

[4] a) J. S. Kasper, P. Hagenmuller, M. Pouchard, C. Cros, *Science* **1965**, *150*, 1713–1714; b) H. G. von Schnering, R. Kröner, W. Carrillo-Cabrera, K. Peters, R. Nesper, *Z. Kristallogr. New Cryst. Struct.* **1998**, *213*, 665–666; c) J. L. Cohn, G. S. Nolas, V. Fessatidis, T. H. Metcalf, G. A. Slack, *Phys. Rev. Lett.* **1999**, *82*, 779–782; d) S. Paschen, W. Carillo-Cabrera, A. Bentien, V. H. Tran, M. Baenitz, Yu. Grin, F. Steglich, *Phys. Rev. B* **2001**, *64*, 214404; e) F. Dubois, T. F. Fässler, *J. Am. Chem. Soc.* **2005**, *127*, 3264–3265; f) W. Carrillo-Cabrera, H. Borrmann, S. Paschen, M. Baenitz, F. Steglich, Yu. Grin, *J. Solid State Chem.* **2005**, *178*, 715–728; g) A. M. Guloy, R. Ramlau, Z. Tang, W. Schnelle, M. Baitinger, Yu. Grin, *Nature* **2006**, *443*, 320–323; h) W. Jung, J. Lörincz, R. Ramlau, H. Borrmann, Yu. Prots, F. Haarmann, W. Schnelle, U. Burkhardt, M. Baitinger, Yu. Grin, *Angew. Chem.* **2007**, *119*, 6846–6850; *Angew. Chem. Int. Ed.* **2007**, *46*, 6725–6728.

[5] K. A. Udachin, G. D. Enright, C. I. Ratcliffe, J. A. Ripmeester, *J. Am. Chem. Soc.* **1997**, *119*, 11481–11486.

[6] S. Bobev, S. C. Sevov, *J. Am. Chem. Soc.* **2001**, *123*, 3389–3390.

[7] H. G. von Schnering, H. Menke, *Angew. Chem.* **1972**, *84*, 30–31; *Angew. Chem. Int. Ed. Engl.* **1972**, *11*, 43–44.

[8] K. A. Kovnir, A. N. Uglov, J. V. Zaikina, A. V. Shevelkov, *Mendeleev Commun.* **2004**, *4*, 135–136.

[9] a) J. V. Zaikina, K. A. Kovnir, R. Demtschyna, U. Burkhardt, Yu. Prots, H. Borrmann, U. Schwarz, A. V. Shevelkov, *The 10th European Conference on Solid State Chemistry*, Book of Abstracts, P096, **2005**, 162; b) J. V. Zaikina, K. A. Kovnir, U. Schwarz, H. Borrmann, A. V. Shevelkov, *Z. Kristallogr. New Cryst. Struct.* **2007**, *222*, 177–179.

[10] a) N. Jaussaud, P. Toulemonde, M. Pouchard, A. San Miguel, P. Gravereau, S. Pechev, G. Goglio, C. Cros, *Solid State Sci.* **2004**, *6*, 401–411; b) N. Jaussaud, M. Pouchard, P. Gravereau, S. Pechev, G. Goglio, C. Cros, A. San Miguel, P. Toulemonde, *Inorg. Chem.* **2005**, *44*, 2210–2214.

[11] E. Reny, S. Yamanaka, C. Cros, M. Pouchard, *Chem. Commun.* **2000**, 2505–2506.

[12] To estimate the tellurium content, *y*, in the clathrate I phase Rietveld refinement was performed by JANA2000 program package (ref. [14]) assuming the composition $Si_{46}Te_y$.

[13] G. M. Sheldrick, *Acta Cryst.* **2008**, *A64*, 112–122.

[14] V. Petricek, M. Dusek, L. Palatinus, *JANA2000*, Institute of Physics, Academy of Science of the Czech Republic **2002**.

[15] The polyhedra are denoted by the number of their faces. The notation $[5^{12}]$ is used for a pentagonal dodecahedron, a 20-vertex polyhedron with 12 pentagonal faces. The 24-vertex and 26-vertex polyhedra containing 12 pentagonal and 2 or 3 hexagonal faces, respectively, are denoted by $[5^{12}6^2]$ or $[5^{12}6^3]$. For notation see F. Liebau, in *Structural Chemistry of Silicates—Structure, Bonding and Classification*; Springer, Berlin, **1985**.
[16] G. K. Ramachandran, P. F. McMillan, J. Dong, Sankey O. F. J. *Solid State Chem.* **2000**, *154*, 626–634.
[17] *Chemistry, Structure and Bonding of Zintl Phases and Ions*; (Ed: S. M. Kauzlarich), VCH, New York, **1996**.
[18] a) K. A. Kovnir, M. M. Shatruk, L. N. Reshetova, I. A. Presniakov, E. V. Dikarev, M. Baitinger, F. Haarmann, W. Schnelle, M. Baenitz, Yu Grin, A. V. Shevelkov, *Solid State Sci.* **2005**, *7*, 957–968; b) *Multinuclear NMR*; (Ed: I. Mason), Plenum Press, New York, **1987**.
[19] Baitinger, M. Ph. D. thesis, Techn. Univ. of Darmstadt, **2000**.
[20] Supporting Information S2: Magnetic susceptibility.
[21] R. T. Sanderson, *Chemical bonds and bond energy*, 2nd Ed. Academic Press, New York, **1976**.
[22] L. G. Akselrud, P. Yu. Zavalii, Yu. Grin, V. K. Pecharsky, B. Baumgartner, E. Wölfel, *Mater. Sci. Forum* **1993**, *133–136*, 335.
[23] W. Schnelle, U. Burkhardt, R. Ramlau, R. Niewa, G. Sparn, *Scientific Report MPI CPfS* **2003**, 38–43.

Received: March 12, 2008
Published online: May 26, 2008

